

## New scintillation ceramics for the X-ray, $\gamma$ - and neutron radiation detectors

© M.V. Korzhik,<sup>1,2</sup> V.M. Retivov,<sup>2</sup> V.V. Dubov,<sup>2</sup> L.V. Ermakova,<sup>2</sup> V.K. Ivanov,<sup>3</sup> P.V. Karpyuk,<sup>2</sup> I.A. Lagutsky,<sup>4</sup> O.Yu. Koval,<sup>2</sup> I.Yu. Komendo,<sup>2</sup> D.E. Lelekova,<sup>2</sup> V.A. Mechinsky,<sup>1,2</sup> V.A. Pustovarov,<sup>5</sup> V.G. Smyslova,<sup>2</sup> P.S. Sokolov,<sup>2</sup> D.N. Tavrunov,<sup>5</sup> A.A. Fedorov<sup>1,2</sup>

<sup>1</sup>S&R Institute of nuclear problems of the Belarussian State University, 220030 Minsk, Republic of Belarus

<sup>2</sup>National Research Center „Kurchatov Institute“, 123182 Moscow, Russia

<sup>3</sup>Kurnakov Institute of General and Inorganic Chemistry, Russian Academy of Sciences, 119071 Moscow, Russia

<sup>4</sup>220005 Minsk, Republic of Belarus

<sup>5</sup>Ural Federal University after the first President of Russia B.N. Yeltsin, 620075 Yekaterinburg, Russia  
e-mail: korjik1064@tut.by

Received September 11, 2024

Revised November 1, 2024

Accepted November 2, 2024

Methods of fabrication and scintillation properties of transparent ceramics of a garnet structure type with a composition of  $(\text{Gd,Me})_3\text{Al}_2\text{Ga}_3\text{O}_{12}$  ( $\text{Me} = \text{Y, Lu}$ ), activated by ions of rare earth elements Ce, Pr, Tb. It is shown that the introduction of a compositional disorder into the cationic sublattice of compounds can significantly improve their scintillation properties. Cumulatively, in terms of their parameters the scintillators  $(\text{Gd, Y})_3\text{Al}_2\text{Ga}_3\text{O}_{12}:\text{Ce, Tb}$  and  $(\text{Gd, Y})_3\text{Al}_2\text{Ga}_3\text{O}_{12}:\text{Ce, Pr}$  exceed  $\text{Gd}_2\text{O}_2\text{S}:\text{Tb, Ce}$ ,  $(\text{Y, Gd})_2\text{O}_2\text{S}:\text{Pr}$  and  $\text{CsI}:\text{Tl}$  for use in the computer tomographic scanners and X-ray scanners. The scintillators  $(\text{Gd, Y, Lu})_3\text{Al}_2\text{Ga}_3\text{O}_{12}:\text{Ce, Mg}$  provide a temporal resolution in matching of the annihilation  $\gamma$ -quanta (511 keV) below 100 ps, which makes them useful for the development of positron-emission tomographs with a possibility of additional selection during the mission. The presence of Gd ions in compounds makes it possible to create neutron counters with detector elements both, as composites and in the form of transparent elements for detecting neutrons in a wide range of the spectrum: from thermal to tens of MeV using both, the amplitude selection and the pulse shape discrimination.

**Keywords:** scintillator, transparent ceramics, garnet, scintillations yield, X-ray scanner, positron-emission tomograph, neutron, rare-earth ions.

DOI: 10.61011/TP.2024.12.60434.271-24

### Introduction

Inorganic scintillation materials are a reliable tool for measuring the ionizing radiation. They are used in a wide range of scanners where penetrating properties of radiation are used, as well as in the scientific research: from measuring the properties of elementary particles to studying the Universe-like elements [1]. Such materials were developed and integrated slightly over a hundred years, while the way was made from the crystalline compounds with a simple di-ionic set in its lattice to the complex cationic and anionic compounds. High-quality multi-ionic crystalline compounds are quite difficult to obtain by extracting from a melt due to the difference in saturated vapors in the growth chamber of various components, as well as the concentration gradient entering the lattice of cations along the axis of growth. An alternative method for producing crystalline scintillators is to fabricate the ceramics using the melt-free method. This method is effective for connections with a cubic space group of

symmetry, which limits the range of potentially suitable connections. Varying the composition of cations in the matrix makes it possible to change sensitivity of the material to various types of ionizing radiation. Thus, it becomes possible to create a set of scintillation materials within the same structural type, which makes it possible to unify technology and significantly reduce the costs during industrial development.

Crystal materials of the garnet structural type based on trivalent cations are the most suitable for this purpose [2]. Such materials based on yttrium and rare earth ions (REI) are, as a rule, radiation-resistant [3–5]. They form a variety of solid solutions during isovalent substitution where isovalent and non-isovalent doping with impurity ions becomes possible. The combination of these properties makes it possible to target and improve the properties of crystalline compounds for use as scintillation materials. In papers [6,7] the application of principle for making more complex the composition of cationic or anionic sublattices in crystalline compounds used for detecting ionizing

radiation is analyzed, primarily to improve the yield of scintillations.

In paper [8], the effect of differences in the ionic potentials of atoms mixed in a cationic lattice is considered, which leads to a violation of the effective potential periodicity in a solid solution and causes its fluctuations. This effect results in a scattering of single-electron states. Fluctuations of the effective potential caused by substitution disorder are described using pseudopotential method [9]. Compositional disorder does not lead to a change in the structural type of the compound or a decrease in the crystal lattice symmetry, i.e. the initial crystallinity is preserved. When replacing cations, it is the anionic sublattice that sustains the long-range order in the arrangement of ions in the lattice. However, as shown in [10,11], the introduction of compositional disorder into the cationic sublattice leads to a significant change in distribution of the electronic states density near the band gap. In most cases, when ionizing radiation interacts with the scintillator substance, ionization occurs in the inner shells of the atoms of the compound. A random track of nonequilibrium charge carriers is formed. In this case, the spatial distribution of the concentration of thermalized nonequilibrium carriers determines the efficiency of electronic excitations energy transfer to an ensemble of radiation centers. Since the excitation of luminescent centers in the compounds under consideration, as a rule, involves formation of exciton states, it is obvious that the final yield of scintillation is determined by the concentration of excitons in the thermalized track. In this case, random modulation of the bottom of the band gap leads to more efficient thermalization of nonequilibrium carriers, primarily electrons. This reduces the volume of the track after thermalization and, as a result, increases the likelihood of exciton formation. Therefore, construction of a material at the atomic level to achieve the track parameters contributing to maximally efficient formation of exciton states of the nonequilibrium carriers has become one of the priorities for further development.

Among the variety of oxide compounds with the garnet structural type, gadolinium-based compounds can be distinguished, the use of which significantly expands the capabilities of controlling scintillation properties, as well as sensitivity to various types of ionizing radiation [12–17].

The oxide compounds based on  $Gd^{3+}$  are featuring multiple  $f$ -levels ( ${}^6P$ ,  ${}^6I$ ,  ${}^6D$ ) in the band gap with formation of subbands. Moreover, from the advanced diagram of electronic states of the trivalent REI [18] it follows that multiple  $f$ -levels of  $Gd^{3+}$  ions in the range of over  $40\,000\text{ cm}^{-1}$  produce a chain of sequential processes including efficient capture of the non-equilibrium carriers with Gd ions and the intracenter relaxation into the lower states  ${}^6P$ ,  ${}^6I$ ; meanwhile, the exchange with the lattice occurs due to both, the auto-localized excitons (ALE) having energy slightly less than the band gap energy, and the Frenkel excitons (FE) localized in  ${}^6P$ ,  ${}^6I$  sub-bands. An increase in compositional disorder due to dilution of the gadolinium sub-lattice, i.e. transition from ternary to quaternary and then penta-cationic

compounds, inevitably leads to violation of gadolinium sub-lattice integrity. Generally, the interaction of the excited configuration  $5d^04f^7$  of  $Gd^{3+}$  ions and their basic configuration  $5d^04f^1$  of  $Ce^{3+}$  activator can be described as an energy transfer of the dipole-dipole interaction. At the same time the jump diffusion over the gadolinium sub-lattice occurs due to the dipole-dipole transfer between  $f$ -states. Thus, energy transfer is a diffusion-controlled dipole-dipole transfer. In a system with disrupted periodicity, the exchange interaction in gadolinium subsystem also becomes higher, therefore, dilution of the gadolinium sub-lattice makes it possible to control both, the yield of scintillations and their kinetics [19].

In this study we've focused on demonstrating the possibilities of control of scintillation parameters of  $(Gd,Me)_3Al_2Ga_3O_{12}$  ( $Me = Y, Lu$ ) compounds activated by Ce, Pr, Tb ions. All compounds are obtained in the form of transparent ceramics, promising for the creation of detector elements, so the laboratory technology for its production can be further scaled to equip domestic scanning equipment.

## 1. Fabrication of transparent ceramics of garnet type compounds

### 1.1. Preparation of precursors

The production of ceramics includes several successive stages, which can be summarized into three: production of a precursor in powder form, its compaction and sintering.

It has been established that the method of precursor co-deposition is optimal for creating transparent ceramics of complex composition. Solid-phase synthesis has also become widespread in the production of pomegranate precursors in the form of powders [20–22]. For aluminum-gallium garnets during preparation, a violation of the compound stoichiometry occurs due to the presence of easily evaporated gallium oxide in the mixture [23], therefore, methods with a short heating time, such as spray pyrolysis, are also applied [24,25]. The disadvantage of the pyrolytic method is the need to obtain regular spherical shape particles (with a narrow dimensional distribution), sometimes hollow inside, which requires continuous pressure application to the powder presses during sintering and makes the equipment expensive in operation. The sol-gel method, including its variation in the form of Pechini method, as well as the method of self-propagating high-temperature synthesis are simple to implement, but difficult to scale and unsuitable for fabrication of garnets due to formation of strong particles agglomerates in them [26–28].

Among the benefits of the co-precipitation method are easy scalability and high chemical homogeneity of a product [29–32]. Fig. 1 illustrates the scanning electron microscopy (SEM) images of GYAGG nano-powder at the treatment temperatures of 850 and 1200°C for 2 h. No powders agglomeration was observed. Thus, the co-precipitation method makes it possible to synthesize weakly

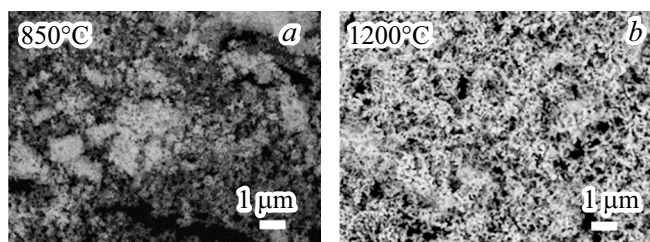


**Figure 1.** SEM images in the mode of back-scattered electrons of GYAGG:Ce nano-powders sintered at thermal treatment temperatures of 850 (a) and 1200°C (b).

agglomerated powders, the structure of which is preserved over a wide temperature range. Such powders are quickly ground to the fractions necessary to obtain blanks for further sintering.

The co-precipitation allows getting the garnet powders with average primary particles size of 50 nm and specific surface of 60–70 m<sup>2</sup>/g. The presence of multiple contacts between them ensures a high sintering capacity, which makes it possible to obtain transparent ceramics without applying pressure.

## 1.2. Powder compaction into a blank for sintering

In ceramic technology, powder compaction is an essential operation. At this stage, the shape and dimensions of the future product are specified. The physical dimensions of the raw material are usually larger than the dimensions of the ceramics being produced. The mechanical properties of the raw material should allow its motion in space during handling for subsequent technological processes. Regardless of the pressing method used, the raw material is usually a composite consisting of an organic binder (mold fixative) and a target dispersed mineral part (inorganic powder). For uniform and non-deformational precipitation during high-temperature sintering of dense ceramics, it is extremely important that the raw material has a uniform density. The homogeneous structure of the raw material is provided during preparation of a liquid slip (suspension) consisting of an inorganic powder, a base medium and various functional additives that stabilize the suspension and minimize the processes of sedimentation and aggregation of particles. In traditional ceramic technology, hot thermoplastic slip casting is often used in cold (usually water-cooled) metal molds. Despite the undeniable advantages of this fabrication method, namely speed and high performance, there is a critical drawback: each prototype of the product usually requires its own unique injection mold, sometimes even a one-time mold, followed by complex mechanical refinement of both, the raw material and the final ceramics.

Conventional method of uniaxial pressing by a hydraulic press with a pressure of 64 MPa was used to seal the precursors. A high-tech method of raw materials fabrication, i.e. a three-dimensional printing, was also used

to produce transparent ceramics of compounds with a garnet structure [33–38]. One of the simplest, relatively cheap and affordable methods is stereolithographic 3D printing or printing in a bathtub using various technical scenarios. It is worth emphasizing that for manufacture of the required raw materials and subsequent ceramic products with architecture of any complexity, the process of layer-by-layer photopolymerization can be implemented in the same bath. The variety of geometric shapes of the created elements is achieved through polymerization of suspension under local illumination using an ultraviolet radiation source or a photoprotector [34–37]. A peculiarity and advantage of stereolithographic 3D printing is the use of widely available acrylate monomers and rheological or dispersing additives produced by hundreds of tons for the modern paint and varnish industry, however, for manufacture of advanced functional ceramics featuring high purity and optical quality, including complex oxides with garnet structure, using stereolithography, it shall be borne in mind that rheological additives can introduce harmful impurities, for example, phosphorus. Such impurities have an adverse effect on the transparency and basic properties of the resulting ceramics [37,38]. Stereolithographic 3D printing makes it possible to produce ceramics of both simple and complex shapes. Samples of compacts made by printing and subsequent annealing and sintering are shown in Fig. 2. Ceramics of complex shapes, including open-work ones, can be used to create detectors of radioactive components of gases and liquids [34], as well as accelerated charged particle beam monitors.

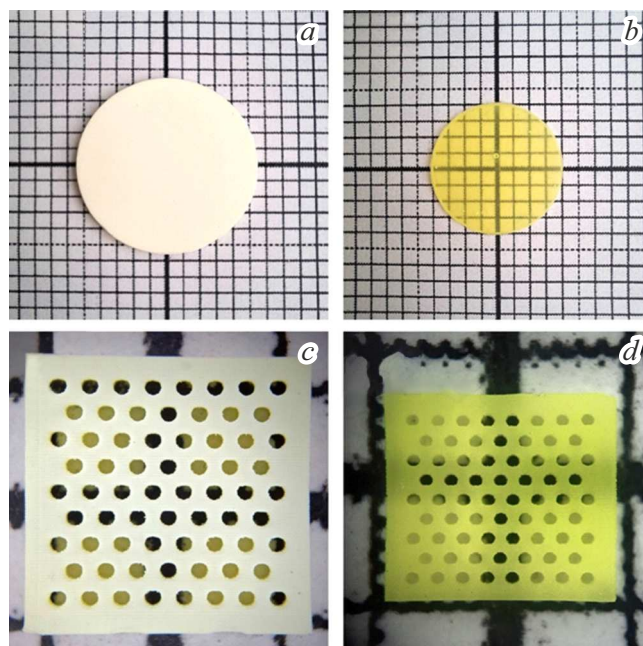


**Figure 2.** Typical view of green products GYAGG:Ce after fabrication on 3D-printer (a, b) and after obtaining a binder from them and high-temperature sintering (c, d) to get a compacted oxide ceramics.

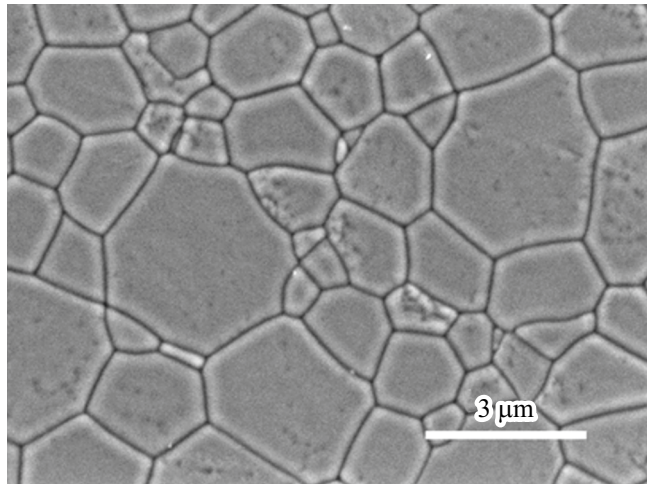


**Figure 3.** SEM image of GYAGG:Ce ceramics obtained by sintering at a temperature of 1700°C during 2 h in oxygen environment.

### 1.3. Sintering to produce transparent ceramics of compounds with a garnet structural type

The main approaches to fabrication of ceramics of high optical transparency are the control of sintering conditions and the introduction of special sintering additives. The sintering conditions include temperature, duration and environment of high-temperature processing of powder compacts. The temperature range of sintering ceramics of garnet compounds, depending on the presence of gallium in the compound, was set in the range from 1600 to 1800°C [39–41]. For the developed compositions of aluminum-gallium garnets, it was found that for raw products from the co-precipitated precursors, the optimal temperature value for obtaining transparent ceramics of three or more cationic compounds lies near 1700°C. When analyzing SEM images of a transect of GYAGG:Ce ceramics obtained by sintering at this temperature, one of which is shown in Fig. 3, we may see almost complete pore yield, and the average grain sized determined by distribution of grain sizes in the transect makes 1.4 μm.

For particles with a highly developed specific surface area used in ceramics manufacture, no stable correlation has been established between the transparency of ceramics and the sintering time.

For the compounds under consideration, sintering in an oxygen atmosphere is optimal. This is confirmed also by the studies of other authors [42,43]. Fig. 4 shows samples of transparent garnet ceramics of various compositions obtained by sintering in an oxygen atmosphere.

The developed technology makes it possible to obtain transparent ceramics of various garnet-type structural compounds containing up to five cations in the crystal lattice.

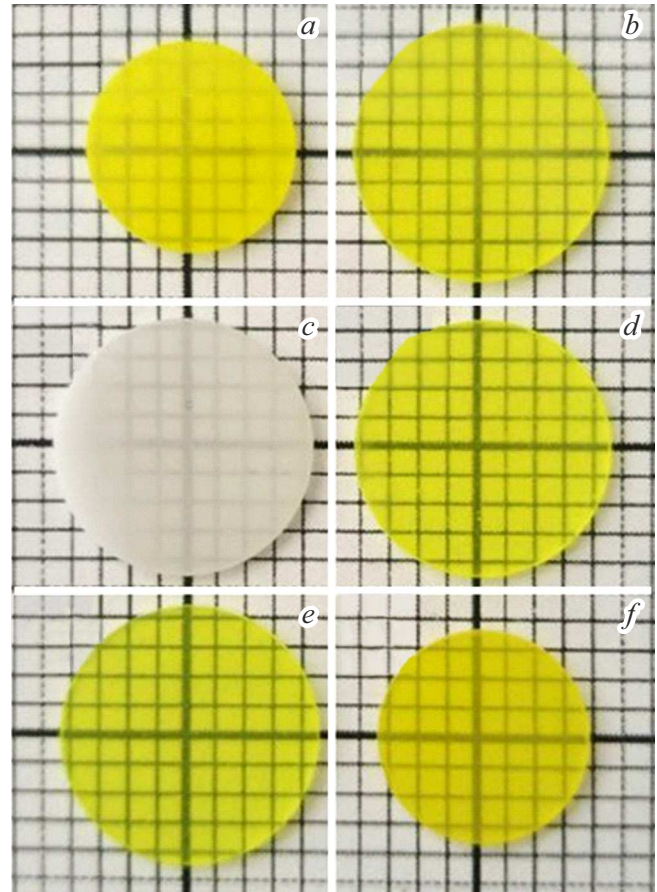


**Figure 4.** Photos of ceramics samples: *a* —  $\text{Gd}_3\text{Al}_2\text{Ga}_3\text{O}_{12}:\text{Ce}$ , *b* —  $(\text{Gd},\text{Y})_3\text{Al}_2\text{Ga}_3\text{O}_{12}:\text{Ce}$ , *c* —  $(\text{Gd},\text{Y})_3\text{Al}_2\text{Ga}_3\text{O}_{12}:\text{Tb}$ , *d* —  $(\text{Gd},\text{Y})_3\text{Al}_2\text{Ga}_3\text{O}_{12}:\text{Ce},\text{Tb}$ , *e* —  $(\text{Gd},\text{Y})_3\text{Al}_2\text{Ga}_3\text{O}_{12}:\text{Ce},\text{Pr}$ , *f* —  $(\text{Gd},\text{Y},\text{Lu})_3\text{Al}_2\text{Ga}_3\text{O}_{12}:\text{Ce},\text{Mg}$  after annealing without additional polishing of surfaces.

## 2. Functional properties of ceramic scintillators

### 2.1. Measurement of the parameters of scintillation ceramics

The scintillations parameters of the developed ceramics samples were measured using various sources of ionizing radiation ( $\alpha$ -,  $\beta$ - and  $\gamma$ -ionization, accelerated electrons) and photodetectors [17,44–47]. When measuring the sensitivity and efficiency of neutrons recording the certified neutron dosimetry ruler Atomtex AT140 based on  $^{238}\text{Pu}$ -Be source was used, as well as the monochromatic neutrons beam with a wavelength of 2.4 Å (14 meV) of the neutron source in the Scientific Center in „Kurchatovsky Institute“.

### 2.2. Materials for X-ray and positron emission scanners

Fabrication of transparent ceramics significantly expands the scope of ceramics application in ionizing radiation

detectors. First of all, we should note the widely used X-ray examination systems (X-ray scanners), which are widespread in medical diagnostics and non-contact examination of people, cargo, flaw detection, etc.

When diagnosing diseases or scanning a person, the use of such devices is associated with exposure to ionizing radiation. The maximum safe radiation dose for humans is 100 mSv per year. In modern systems the effective exposure dose for a human generally makes  $0.25 \mu\text{Sv}$  [48] per session, and, hence, exclude the routine screening of more than once a day. Therefore, the development of low-dose X-ray examination systems that allow safe human screening at least 1000 times a year is the most promising strategy for security check systems.

The choice of detector materials is determined by the type of X-ray source and the method of signal processing in X-ray scanners (XR) or computer tomographs (CT). We should highlight such materials as  $\text{Gd}_2\text{O}_2\text{S:Tb}$ ,  $(\text{Y,Gd})_2\text{O}_2\text{S:Pr}$ ,  $\text{Gd}_2\text{O}_2\text{S:Tb}$ , Ce as the commonly used in the majority of foreign CT [49–51]. Energy integration detectors (EID) are widely used. When using scintillators in such scanners, the photodetector current from the stream of optical photons generated in the scintillator is recorded. EID measure the energy-integrated signals of absorbed X-ray quanta, thus losing all energy-dependent information. In addition, electronic noise is additionally integrated in EID, which leads to lower image contrast. The further development of EID-equipped devices became the scanners where two X-ray energies are used, which required two-layer detectors optimized for soft and harder X-rays. For such an application, the main parameters of scintillators are the scintillations yield and the minimum level of phosphorescence of the material in the illuminated light sum.

The further development of X-ray tube technology and heavy semiconductor materials has made the detection of individual X-ray quanta (DIQ) relevant, which provides undeniable advantages for medical and security check systems [52,53], as it provides measurements in an optimal signal-to-noise pulse mode. Because of this, known samples of such scanners based on cadmium-zinc-tellurium (CZT) semiconductor detectors are superior to the traditional EID-based CTs in all respects: reduced dose load on a patient, image quality and contour sharpness of soft tissues and bones, noise and the presence of image processing artifacts [54–56]. At the same time, the limited availability of CZT on the market has stimulated interest in using scintillation meters in DIQ. Among the essential requirements to DIQ-based detectors are the following: possibility to create pixels of a size from  $0.5 \times 0.5$  to  $1 \times 1$  mm, maximal counting speed per pixel from  $1 \cdot 10^6 \text{ s}^{-1}$  to  $5 - 7 \cdot 10^6 \text{ s}^{-1}$ , which is technically feasible with the use of scintillation materials based on the cutting-edge semiconductor photodetectors.

A comparison of the parameters of the developed scintillators with those used in various modifications of X-ray and CT scanners is given in the table 1, and Figure 5 shows a linear detector module made of GYAGG:Tb,Ce pixels, and a

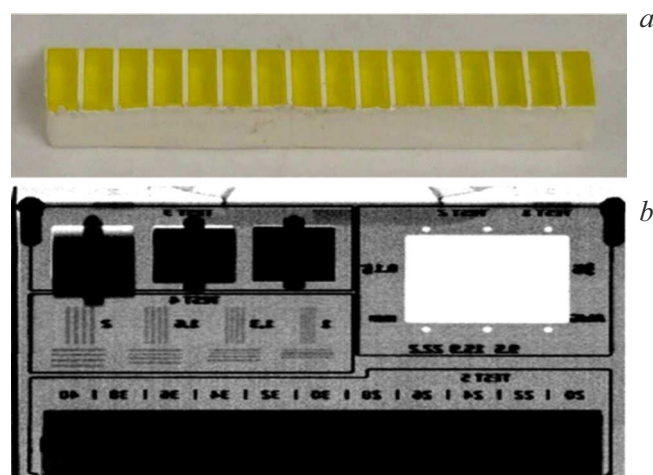


**Figure 5.** Photo of a 1x16 linear element made of GYAGG:Tb,Ce ceramics for use in the absorbed X-ray quanta energy integration detectors in RS (a) and a test image obtained in the scanner with detector module containing four elements (b).

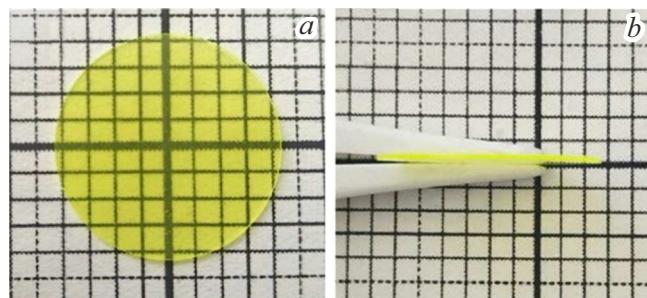


**Figure 6.** Image of ceramic element GYAGG:Ce,Tb with a thickness of  $200 \mu\text{m}$  on flat surface (a) and perpendicular to it (b).

test image obtained using a detector module based on four linear elements.

We see that materials based on GYAGG:Tb,Ce ceramics [44] for creation of EID-based detectors have a benefit in terms of scintillations yield compared to GOS:Tb materials, and GYAGG:Pr,Ce ceramic materials — have benefits compared to GOS:Pr,Ce,F. Due to transparency of the fabricated ceramics it became possible to use thicker layers without significant loss of scintillation yield, which compensates for the lower absorption capacity of X-ray radiation compared to gadolinium oxysulfide. For DIQ-based scanners the developed materials provide an order of magnitude higher loads than CZT semiconductor converters.

In a low-energy X-ray scanner, it is possible to use thin plates of a ceramic scintillator. Fig. 6 illustrates an element of GYAGG:Tb,Ce ceramics with a thickness of  $200 \mu\text{m}$ , which, when measured at S&R Center in „Kurchatov Institute“ provided a spatial resolution of higher than  $60 \mu\text{m}$ . The possibility of manufacturing thin samples confirms the high quality of ceramics, the yield of suitable elements during machining is more than 80%.

**Table 1.** Parameters of scintillators Gd<sub>2</sub>O<sub>2</sub>S:Tb, Gd<sub>2</sub>O<sub>2</sub>S:Pr,Ce,F CsI(Tl) compared with data provided in this paper for use in the X-ray scanners and computer tomographs. Data of GOS family ceramics are given in [49]

Application area	Scanners with DIQ-based detectors			Scanners with EID-based detectors			
Material	GAGG:Ce	GYAGG:Ce	GYAGG:Tb,Ce	GYAGG:Pr,Ce	GOS:Pr,Ce,F	GOS:Tb	CsI(Tl)
Form of material	Monocrystal, ceramics	Monocrystal, ceramics	Monocrystal, ceramics	Monocrystal, ceramics	Ceramics	Ceramics	Monocrystal
Position of the maximum luminescence [nm]	520	520	546	530	520	546	550
Relative light yield	0.7 (20°C) 0.9 (-25°C)	0.9 (20°C)	1.6 (20°C)	0.7	0.5	0.9	1
Scintillation decay system [μs]	0.08	0.05	0.06 (40%) 2000 (60%)	0.08 (90%) 0.5 (10%)	3	3000	0.6
Phosphorescence after 30 ms [%]	< 0.1	< 0.1	< 0.1	< 0.1	< 0.1	< 0.1	1.5
Transparency	Transparent	Transparent	Transparent	Transparent	Semi- Semi-transparent	Transparent transparent	
Density	6.68	5.86	5.86	5.86	7.34	7.34	4.53
Hygroscopic property	no	no	no	no	no	no	average

**Table 2.** Scintillation materials for PET scanners

Material	Density, g/cm <sup>3</sup>	Z <sub>eff</sub> /absorption coefficient for 511 keV, cm <sup>-1</sup>	Light yield, phot./MeV	τ <sub>sc</sub> , ns	λ <sub>max.sc</sub> , nm	Temporal resolution of coincidence, ps
Bi <sub>3</sub> Ge <sub>4</sub> O <sub>12</sub> (BGO)	7.13	75.2/0.37	8 200	300	505	550
Lu <sub>2</sub> SiO <sub>5</sub> :Ce (LSO)	7.4	66/0.28	27 000	40	420	115(20°C) 117(0°C) 121(-20°C)
(Lu,Y) <sub>2</sub> SiO <sub>5</sub> :Ce (LYSO)	7.0	62/0.21	30 000	35	420	93(20°C) 95(0°C) 104(-20°C)
(Gd,Y,Lu) <sub>3</sub> Al <sub>2</sub> Ga <sub>3</sub> O <sub>12</sub> :Ce,Mg (GYLAGG:Ce)	6.7	52/0.13	41 000	14(84%) 78(16%)	520	97(20°C) 95(0°C) 93(-20°C)

In addition to CT scanners, PET (positron emission tomographs) scanners have become widespread in today's medical diagnostics. Currently, in PET scanners the scintillation materials are used as detectors; the technique of recording the annihilation γ-quanta (511 keV) was properly developed based on a coincidence method [57,58]. In details, the scintillators and their application are outlined in paper [1].

High stopping power, high energy resolution, low after-glow level and good temporal resolution of coincidences are a necessary set of parameters for the application of scintillation material in PET. Table. 2 gives a comparison of properties of the scintillation materials used in PET-scanners with GYLAGG:Ce material described in this paper [46]. Also temporal resolution of coincidences obtained from laboratory samples with dimensions 3 × 3 × (2 – 5) mm

and commercial silicon photomultipliers (SiPM) at various temperatures are compared. The accuracy of coincidence temporal resolution (CTR) was  $\pm 2$  ps.

An essential requirement for better sensitivity is high CTR to provide efficient use of Time-of-Flight (TOF) approach for recording the annihilation  $\gamma$ -quanta. The improved  $G$ -values of signal-to-noise ratio (SNR) with the use of TOF and without it CTR:

$$G = \sqrt{\frac{SNR_{TOF}}{SNR_{nonTOF}}} = \sqrt{\frac{2D}{c \cdot CTR}}, \quad (1)$$

where  $c$  — speed of light. Assuming that a patient is 40 cm in diameter ( $D$ ) the signal-to-noise ratio (SNR) improvement factor may reach 2.3 and 5.2 for resolution of CTR 500 and 100 ps, respectively.

BGO material was used in first-generation scanners and is now actively used in low-cost scanners, for example, those manufactured by General Electric (USA). Modern BGO-based PET-scanners have a temporal resolution (FWHM) from 550 to 650 ps. Using TOF allows improving the reconstructed signal-to-noise ratio of the image by about two times compared to standard PET scanners without TOF.

In the detector part of PET-scanners a transition to SiPM is underway. Their disadvantage is the relatively high intrinsic noise, which, however, can be reduced by lowering the temperature. In the detector based on the scintillator presented in this paper, a significant improvement in time resolution is observed with a decrease in temperature. This is due to the fact that with a decrease in temperature in gadolinium-aluminum-gallium garnets, the yield of scintillations increases [59]. For the same reason, there is an improvement in energy resolution.

### 2.3. Measurement of neutrons from radioisotope sources

The results of measurements using a neutron dosimeter ruler are shown in Fig. 7 and correlate well with the response spectra of GAGG:Ce single crystals to neutrons [17]. The amplitude spectrum  $I$  was obtained in a straight beam of fast neutrons with a flow of 223.0 neutron/(s·cm<sup>2</sup>) without any material between the source and the detector.

Spectrum 2 was obtained with the use of retarder placed in front of the source <sup>238</sup>Pu-Be. The amplitude spectrum of 3 was measured using a retarder and a cadmium filter installed in front of the source. All spectra are presented after subtracting the contribution of the natural background, the accumulation times of the spectra were 600 s, including the spectrum of the natural background. Spectrum 4 is obtained by subtracting spectrum 3 from spectrum 2 and represents the spectrum of neutron recording in the energy range from 0.0253 to 0.4 eV at a flux of 25.0 neutron/(s·cm<sup>2</sup>) at the measuring point. It can be seen that the material has good sensitivity also in the field of above-thermal neutrons.

The calculated values of sensitivity and detection efficiency for various energy ranges of gamma quanta formed

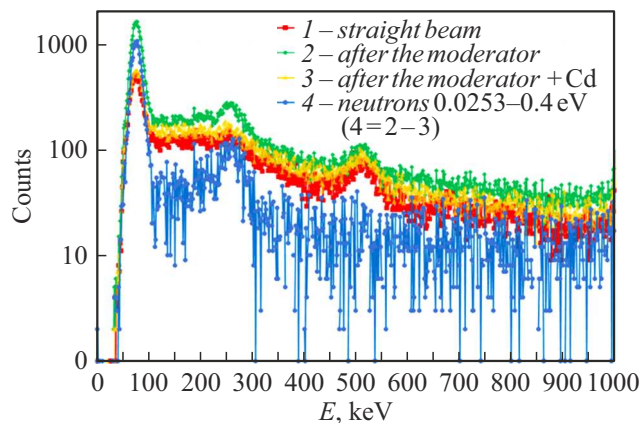


**Figure 7.** Amplitude spectra measured at the test stand with <sup>238</sup>Pu-Be source.

in the scintillator during interaction with neutrons, starting from 45 keV, are listed in Table 3. The sensitivity was calculated from the sum of the samples in the range of energies, known fluxes, and accumulation time.

In the bottom of Table 3 the neutron equivalents of the counting speeds were summed up from natural background 0.1  $\mu$ Sv/h and from Co-60 at power of exposure dose of 1.0  $\mu$ Sv/h. The data were obtained in normal conditions at a room temperature of (300 K). The total (main and additional) errors for the sensitivity and efficiency results for fast neutrons are estimated as not exceeding  $\pm 5\%$ . The sources of this error are mainly statistical errors, errors in determining the flow and positioning of the detector.

The main and additional measurement errors for the neutron equivalents of counting speeds from the natural background 0.1  $\mu$ Sv/h didn't exceed  $\pm 22\%$  for the range of energies 45–10<sup>5</sup> keV and  $\pm 12\%$  - for the rest ones, including a total inaccuracy contribution of the system's verification dosimeter and statistical error in the obtained spectrum. The total error for the neutron equivalents of the counting speeds from Co-60 did not exceed  $\pm 6\%$ , including the RMS statistical error of the dose power and the uncertainty of positioning.

The developed detector demonstrates high sensitivity to fast neutrons. Using a retarder further improves the sensitivity. At the same time, the neutron equivalents of the counting speeds from Co-60 and even from the natural background are relatively high. It should be noted here that for a thermal neutron detector, the thickness can be significantly reduced (up to 0.1–0.2 mm) without a critical loss of sensitivity to neutrons (almost 45% of useful neutron counts (Table. 3) are concentrated in a group of lines with a maximum near 80 keV, which is itself a superposition of lines of characteristic X-ray radiation and an internal conversion electron with approximately equal energy, for which the effective path length in GYAGG does not exceed 50–100  $\mu$ m).

During interaction of neutrons with an energy of more than 8 MeV with GYAGG substance the secondary charged

**Table 3.** Rated sensitivity and efficiency of recording of various energy ranges of  $\gamma$ -quanta formed in the detector material reduced to the detector thickness of 1 cm, when interacting with neutrons; neutron equivalents of the count speed from the natural background of  $0.1 \mu\text{Sv/h}$  and Co-60  $1.0 \mu\text{Sv/h}$

Energy range of gamma-quanta, keV	Fast neutrons		Slow neutrons	
	Sensitivity, pulse per second per 1 neutron/(s·cm <sup>2</sup> )	Efficiency recording of neutrons, %	Sensitivity, pulse per second per 1 neutron/(s·cm <sup>2</sup> )	Efficiency recording of neutrons, %
45 – 105	0.073	3.74	1.14	44.9
45–305	0.182	9.29	1.64	64.6
45–550	0.247	12.6	1.80	71.0
45–1000	0.298	15.2	2.04	80.3

Energy range gamma-quanta, keV	Fast neutrons		Slow neutrons	
	Neutron equivalent counting speed from natural background $0.1 \mu\text{Sv/h}$ , neutron/(s·cm <sup>2</sup> )	Neutron equivalent counting speed from Co-60 $1.0 \mu\text{Sv/h}$ , neutron/(s·cm <sup>2</sup> )	Neutron equivalent counting speed from natural background $0.1 \mu\text{Sv/h}$ , neutron/(s·cm <sup>2</sup> )	Neutron equivalent counting speed from Co-60 $1.0 \mu\text{Sv/h}$ , neutron/(s·cm <sup>2</sup> )
45–105	2.07	10.6	0.133	0.679
45–305	3.85	21.6	0.428	2.39
45–550	4.40	25.2	0.603	3.45
45–1000	4.86	31.1	0.709	4.55

particles are generated here,  $\alpha$ -particles and protons. As shown in jcite60, the spectrum of fast neutrons is separated by the shape of the pulse from the background  $\gamma$ radiation.

### 2.4. Screen type detectors

Composite detectors based on the developed materials can be used to create composite detector elements of the screen type. In this case, transparent ceramics can be ground into a powder with a given granulometric composition, and both a transparent polymerizable binder and an additional neutron absorber in the form of <sup>6</sup>LiF powder can be added to the composite. Unlike ZnS(Ag) scintillator used in such composites, ceramic particles retain optical transparency, which contributes to a better light collection of the composite.

The amplitude spectra of composite samples containing lithium fluoride of natural origin were obtained using a source of  $\alpha$ particles <sup>241</sup>Am ( $10^4$  Bq) using the technique described in [61]. Figure 8 shows a comparison of the response from samples made from ceramic GYAGG scintillator powder. To measure the scintillations yield from the surface of sample the composite was saturated with garnet powder,  $\sim 90\%$  by volume, which provided density of  $\sim 50 \text{ mg/cm}^2$ . As a reference sample for comparison a fragment of neutron screen Scintacor ND  $12 \times 12$  mm (ND-screen) was used. The measurements were carried out using HAMAMATSU R329 photoelectron multiplier

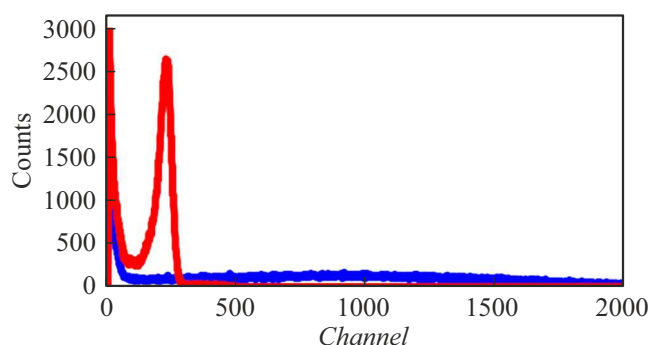


**Figure 8.** Amplitude spectra of a screen made on the basis of a powder from a ceramic GYAGG scintillator (red curve) and a comparison sample (blue curve).

inclined at an angle of  $45^\circ$  to the source surface irradiated by  $\alpha$  particles.

The GYAGG-based sample showed a clearly discernible peak of total absorption of  $\alpha$ particles, which is in principle unattainable using a screen based on opaque ZnS(Ag) particles. This allows for amplitude selection when registering both charged particles and neutrons.

To measure the spatial resolution during neutron detection, samples were prepared using <sup>6</sup>LiF (90% enrichment). The screen coating included a scintillator, lithium fluoride, and a binder. The thickness layer was below  $30 \text{ mg/cm}^2$ .

**Table 4.** The results of measurements of the spatial resolution of samples and parameters of their scintillation kinetics

Screen sample	Measured spatial resolution with system of counting, $\mu\text{m}$	Rated intrinsic spatial screen resolution, $\mu\text{m}$	Decay time kinetics scintillations, s
Compared sample GOS(Tb)	$202 \pm 5.0$	$52.7 \pm 7.1$	$2 \times 10^{-3}$
Compared sample ZnS(Ag)/ $^6\text{LiF}$	$220 \pm 5.2$	$101.9 \pm 7.2$	$4.5 \times 10^{-6}$
GYAGG:Ce (30 vol.%) LiF (30 vol.%) Binder (40 vol.%)	$216 \pm 5.1$	$92.9 \pm 7.1$	$80 \times 10^{-9}$
GYAGG:Tb (23 vol.%) LiF(73 vol.%) Binder (4 vol.%)	$212 \pm 5.1$	$81.2 \pm 7.1$	$2 \times 10^{-3}$

The eigen spatial resolution of the counting system on a neutron source in R&D Center at „Kurchatov Institute“ was  $195 \pm 5.0 \mu\text{m}$ . The screens GOS(Tb) and ZnS(Ag)/ $^6\text{LiF}$  with a thickness of 46 and  $100 \mu\text{m}$ , respectively, were used as reference samples for comparison.

The spatial resolution was measured by installing a slit cadmium mask in front of the composite, the size of one pixel of the optical system was  $65 \mu\text{m}$ . Measurements of spatial resolution of the samples and the parameters of their scintillation kinetics are presented in Table 4.

The spatial resolution of the screen samples based on the developed materials exceeds that of ZnS(Ag)/ $^6\text{LiF}$  and approaches that obtained with GOS(Tb). The duration of the scintillation pulse in the developed GYAGG-based screen sample containing Ce is 25,000 times shorter than that of GOS(Tb) reference sample, and 55 times shorter than that of ZnS(Ag)/ $^6\text{LiF}$  reference sample. The speed of statistics collection, and, consequently, the measurement performance, increases accordingly.

## Conclusion

An original technology for producing transparent ceramic scintillation materials with a garnet structural type has been developed. Scintillators  $(\text{Gd},\text{Y})_3\text{Al}_2\text{Ga}_3\text{O}_{12}:\text{Ce}$ ,  $(\text{Gd},\text{Y})_3\text{Al}_2\text{Ga}_3\text{O}_{12}:\text{Tb},\text{Ce}$  and  $(\text{Gd},\text{Y})_3\text{Al}_2\text{Ga}_3\text{O}_{12}:\text{Ce},\text{Pr}$  may be used in X-ray scanners for various purposes; at that, these scintillators are capable of providing high performance characteristics both in detectors with integrated response to absorbed X-ray energy and with measurement of its individual quanta.

Scintillator  $(\text{Gd},\text{Y},\text{Lu})_3\text{Al}_2\text{Ga}_3\text{O}_{12}:\text{Ce},\text{Mg}$  may replace scintillators  $(\text{Lu},\text{Y})_2\text{SiO}_5:\text{Ce}$  (according to its parameters) in the detector sections of positron emission scanners, while the achieved time resolution of coincidences with detectors made of this material makes it possible to effectively use the time-of-flight TOF technique for the annihilation  $\gamma$  quanta. The material can be made in the form of plates with a thickness of 3 – 4mm and used with minimal loss of

crystalline mass during machining to create pixel elements for matrix detector modules.

The presence of gadolinium atoms in the developed materials also makes them applicable in recording of neutrons in a wide range of their energies and in various detector designs.

## Funding

The samples of materials were fabricated in the S&R Center of „Kurchatov Institute“ supported by the Ministry of Science and Higher Education of Russia, agreement № 075-15-2021-1353 dated October 12, 2021. The analytical studies were carried out using the scientific equipment of the Collective Use Center at „Research Chemical-Analytical Center of S&R Center at „Kurchatov Institute“. The authors from the Ural Federal University express their thanks to the Ministry of Science and Higher Education of Russia for support within the project FEUZ-2023-0013.

## Conflict of interest

The authors declare that they have no conflict of interest

## References

- [1] P. Lecoq, A. Gektin, M. Korzhik. *Inorganic Scintillators for Detector Systems; Particle Acceleration and Detection* (Springer International Publishing, Cham, 2017)
- [2] G. Zhang, Y. Wu. *Int. J. Appl. Ceram. Technol.*, **19**, 664 (2022). DOI: 10.1111/ijac.13856
- [3] E. Auffray, A. Fedorov, V. Dormenev, J. Houžvička, M. Korjik, M.T. Lucchini, V. Mechinsky, S. Ochesanu. *Nucl. Instrum. Meth. Phys. Res. A*, **856**, 7 (2017). DOI: 10.1016/j.nima.2016.09.037
- [4] E. Auffray, G. Dosovitskiy, A. Fedorov, I. Guz, M. Korjik, N. Kratochwill, M. Lucchini, S. Nargelas, D. Kozlov, V. Mechinsky. *Radiat. Phys. Chem.*, **164**, 108365 (2019). DOI: 10.1016/j.radphyschem.2019.108365

- [5] V. Alenkov, O. Buzanov, G. Dosovitskiy, V. Egorychev, A. Fedorov, A. Golutvin, Yu. Guz, R. Jacobsson, M. Korjik, D. Kozlov, V. Mechinsky, A. Schopper, A. Semennikov, P. Shatalov, E. Shmanin. *Nucl. Instrum. Meth. Phys. Res. A*, **916**, 226 (2019). DOI: 10.1016/j.nima.2018.11.101
- [6] V. Retivov, V. Dubov, I. Komendo, P. Karpyuk, D. Kuznetsova, P. Sokolov, Y. Talochka, M. Korzhik. *Nanomaterials*, **12**, 4295 (2022). DOI: 10.3390/nano12234295
- [7] D. Zhu, M. Nikl, W. Chewpraditkul, J. Li. *J. Adv. Ceram.*, **11**, 1825 (2022). DOI: 10.1007/s40145-022-0660-9
- [8] Y. Talochka, A. Vasil'ev, M. Korzhik, G. Tamulaitis. *J. Appl. Phys.*, **132**, 053101 (2022). DOI: 10.1063/5.0098905
- [9] J.R. Cárdenas. *Superlattices Microstruct.*, **100**, 548 (2016). DOI: 10.1016/j.spmi.2016.10.009
- [10] A.V. Gektin, A.N. Belsky, A.N. Vasil'ev. *IEEE Trans. Nucl. Sci.*, **61**, 262 (2014). DOI: 10.1109/TNS.2013.2277883
- [11] M. Korzhik, G. Tamulaitis, A.N. Vasil'ev. *Physics of Fast Processes in Scintillators; Particle Acceleration and Detection* (Springer International Publishing, Cham, 2020)
- [12] K. Kamada, T. Endo, K. Tsutumi, T. Yanagida, Y. Fujimoto, A. Fukabori, A. Yoshikawa, J. Pejchal, M. Nikl. *Cryst. Growth Des.*, **11**, 4484 (2011). DOI: 10.1021/cg200694a
- [13] K. Kamada, S. Kurosawa, P. Prusa, M. Nikl, V. Kochurikhin, T. Endo, K. Tsutumi, H. Sato, Y. Yokota, K. Sugiyama, A. Yoshikawa. *Opt. Mater.*, **36** (12), 1942 (2014). DOI: 10.1016/j.optmat.2014.04.001
- [14] M. Korzhik, V. Alenkov, O. Buzanov, G. Dosovitskiy, A. Fedorov, D. Kozlov, V. Mechinsky, S. Nargelas, G. Tamulaitis, A. Vaitkevicius. *Cryst. Eng. Comm.*, **22**, 2502 (2020). DOI: 10.1039/D0CE00105H
- [15] K. Omuro, M. Yoshino, K. Bartosiewicz, T. Horiai, R. Murakami, K.J. Kim, K. Kamada, R. Kucerkova, V. Babin, M. Nikl, A. Yamaji, T. Hanada, Y. Yokota, S. Kurosawa, Y. Ohashi, H. Sato, A. Yoshikawa. *J. Lumin.*, **273**, 120663 (2024). DOI: 10.1016/j.jlumin.2024.120663
- [16] W. Chewpraditkul, N. Pattanaboonmee, W. Chewpraditkul, T. Szczesniak, M. Moszynski, K. Kamada, A. Yoshikawa, R. Kurcerava, M. Nikl. *Nucl. Instrum. Meth. Phys. Res. A*, **1004**, 165381 (2021). DOI: 10.1016/j.nima.2021.165381
- [17] M. Korjik, K.-T. Brinkmann, G. Dosovitskiy, V. Dormenev, A. Fedorov, D. Kozlov, V. Mechinsky, H.-G. Zaunick. *IEEE Trans. Nucl. Sci.*, **66** (1), 536 (2018).
- [18] T. Wegh, A. Meijerink, R.-J. Lamminmaki, J. Holsa. *J. Lumin.*, **87–89**, 1002 (2000). DOI: 10.1016/S0022-2313(99)00506-2
- [19] M. Korzhik, V. Retivov, A. Bondarau, G. Dosovitskiy, V. Dubov, I. Kamenskikh, P. Karpuk, D. Kuznetsova, V. Smyslova, V. Mechinsky, V. Pustovarov, D. Tavruncov, E. Tishchenko, A. Vasil'ev. *Crystals*, **12**, 1196 (2022). DOI: 10.3390/cryst12091196
- [20] X. Chen, H. Qin, Y. Zhang, Y. Liu, J. Jiang, H. Jiang. *Opt. Mater. Express.*, **6** (2), 610 (2016). DOI: 10.1364/OME.6.000610
- [21] H. Wiecezorek, V. Khanin, C. Ronda, J. Boerekamp, S. Spoor, R. Steadman, I. Venetsev, K. Chernenko, T. Tukhvatulina, I. Vrubel, A. Meijerink, P. Rodnyi. *IEEE Trans. Nucl. Sci.*, **67** (8), 1934 (2020). DOI: 10.1109/TNS.2020.3001303
- [22] X. Li, D.H. Hu, Y.Z. Ma, Q.E. Sa, X.R. Wang, F.X. Wang, Z.Q. Song, K.F. Chao. *Sol. St. Phen.*, **323**, 66 (2021). DOI: 10.4028/www.scientific.net/SSP.323.66
- [23] R.H. Lamoreaux, D.L. Hildenbrand, L. Brewer. *J. Phys. Chem. Ref. Data.*, **16** (3), 419 (1987). DOI: 10.1063/1.555799
- [24] N. Sakar, H. Gergeroglu, S.A. Akalin, S. Oguzlar, S. Yildirim. *Opt. Mater.*, **103**, 109819 (2020). DOI: 10.1016/j.optmat.2020.109819;
- [25] J. Marchal, T. John, R. Baranwal, T. Hinklin, R.M. Laine. *Chem. Mater.*, **16** (5), 82 (2004). DOI: 10.1021/cm021783l
- [26] P. Głuchowski, R. Tomala, R. Kowalski, O. Ignatenko, M.E. Witkowski, W. Drozdowski, W. Stręk, W. Ryba-Romanowski, P. Solarz. *Ceram. Int.*, **45** (17), 21870 (2019). DOI: 10.1016/j.ceramint.2019.07.197
- [27] J. Li, Y. Pan, F. Qiu, Y. Wu, J. Guo. *Ceram. Int.*, **34** (1), 141 (2008). DOI: 10.1016/j.ceramint.2006.09.002
- [28] M.P. Pechini. US Patent 3,3306,97 (1967)
- [29] X. Zhang, G. Yang, R. Chi, Y. Shi, X. Zhao, H. Jiang, F. Guo, G. Wang, J. Guo, Z. Zhang. *Int. J. Appl. Ceram. Tech.*, **19** (5), 2419 (2022). DOI: 10.1111/ijac.14084
- [30] Z. Hu, X. Chen, X. Liu, X. Li, T. Xie, Y. Shi, H. Kou, Y. Pan, E. Mihóková, M. Nikl, J. Li. *J. Alloy. Compd.*, **818**, 152885 (2020). DOI: 10.1016/j.jallcom.2019.152885
- [31] D. Sun, Q. Zhang, Z. Wang, J. Su, C. Gu, A. Wang, S. Yin. *Mat. Sci. Eng. A*, **392** (1–2), 278 (2005). DOI: 10.1016/j.msea.2004.09.057
- [32] Y. Sun, S. Yang, Y. Zhang, J. Jiang, H. Jiang. *IEEE Trans. Nucl. Sci.*, **61** (1), 306 (2014). DOI: 10.1109/TNS.2013.2291320
- [33] G.A. Dosovitskiy, P.V. Karpyuk, P.V. Evdokimov, D.E. Kuznetsova, V.A. Mechinsky, A.E. Borisovich, A.A. Fedorov, V.I. Putlayev, A.E. Dosovitskiy, M.V. Korjik. *Cryst. Eng. Comm*, **19**, 4260 (2017). DOI: 10.1039/C7CE00541E
- [34] A.A. Fedorov, V.V. Dubov, L.V. Ermakova, A.G. Bondarev, P.V. Karpyuk, M.V. Korzhik, D.E. Kuznetsova, V.A. Mechinsky, V.G. Smyslova, G.A. Dosovitskiy, P.S. Sokolov. *Instrum. Exp. Tech.*, **66**, 234 (2023). DOI: 10.1134/S002044122301013X
- [35] L.V. Ermakova, V.V. Dubov, R.R. Saifutayarov, D.E. Kuznetsova, M.S. Malozovskaya, P.V. Karpyuk, G.A. Dosovitskiy, P.S. Sokolov. *Ceramics*, **6**, 43 (2024). DOI: 10.3390/ceramics6010004
- [36] L.V. Ermakova, V.G. Smyslova, V.V. Dubov, P.V. Karpyuk, P.S. Sokolov, I.Yu. Komendo, A.G. Bondarau, V.A. Mechinsky, M.V. Korzhik. *Photonisc*, **11**, 685 (2024). DOI: photonisc11080695
- [37] L.V. Ermakova, V.G. Smyslova, V.V. Dubov, D.E. Kuznetsova, M.S. Malozovskaya, R.R. Saifutayarov, P.V. Karpyuk, P.S. Sokolov, I.Yu. Komendo, A.G. Bondarau, V.A. Mechinsky, M.V. Korzhik. *Ceramics*, **6**, 1478, (2023). DOI: 10.3390/ceramics6030091
- [38] P.V. Karpyuk, L.V. Ermakova, V.V. Dubov, D.E. Lelekova, R.R. Saifutayarov, P.A. Zhdanov, M.S. Malozovskaya, I.Yu. Komendo, P.S. Sokolov, A.G. Bondarau, M.V. Korzhik, *J. Surf. Invest. X-ray.*, **18**, 983 (2024). DOI: 10.1134/S1027451024700733
- [39] Z. Luo, H. Jiang, J. Jiang, R. Mao. *Ceram. Inter.*, **41** (1), 873 (2015). DOI: 10.1016/j.ceramint.2014.08.137
- [40] Z.M. Seeley, N.J. Cherepy, S.A. Payne. *J. Cryst. Growth.*, **379**, 793 (2013). DOI: 10.1016/j.jcrysgro.2012.11.042
- [41] Q. Yao, L. Zhang, P. Gao, B. Sun, C. Shao, Y. Ma, T. Zhou, M. Li, H. Chen, Y. Wang. *J. Am. Ceram. Soc.*, **103** (6), 3513 (2020). DOI: 10.1111/jace.17052
- [42] S. Chen, B. Jiang, Q. Zhu, W. Ma, G. Zhang, Y. Jiang, W. Chewpraditkul, L. Zhang. *Nucl. Instrum. Meth. Phys. Res. A.*, **942**, 162360 (2019). DOI: 10.1016/j.nima.2019.162360

- [43] X. Qiu, Z. Luo, J. Zhang, H. Jiang, J. Jiang. *Ceram. Inter.*, **46** (4), 4550 (2020). DOI: 10.1016/j.ceramint.2019.10.183
- [44] M. Korzhik, P. Karpyuk, A. Bondarau, A. Ilyushin, I. Kamenskikh, D. Lelekova, V. Pustovarov, V. Retivov, V. Smyslova, D. Tavrnov, A. Vasil'ev. *J. Lumin.*, **265**, 120226 (2024). DOI: 10.1016/j.jlumin.2023.120226
- [45] M. Korzhik, R. Abashev, A. Fedorov, G. Dosovitskiy, E. Gordienko, I. Kamenskikh, D. Kazlou, D. Kuznecova, V. Mechinsky, V. Pustovarov, V. Retivov, A. Vasil'ev. *Nucl. Eng. Technol.*, **54** (7), 2579 (2022). DOI: 10.1016/j.net.2022.02.007
- [46] M. Korzhik, V. Dubov, M. Bazalevsky, A. Bondarau, O. Buzanov, D. Lelekova, P. Karpuk, Vi. Mechinsky, V. Vasiliev, D. Yanushevich. *Opt. Mater.*, **151**, 115334 (2024). DOI: 10.1016/j.optmat.2024.115334
- [47] P. Karpyuk, M. Korzhik, A. Fedorov, I. Kamenskikh, I. Komendo, D. Kuznetsova, E. Leksina, V. Mechinsky, V. Pustovarov, V. Smyslova, V. Retivov, Y. Talochka, D. Tavrnov, A. Vasil'ev. *Appl. Sci.*, **13**, 3323 (2023). DOI: 10.3390/app13053323
- [48] STATEMENT OF THE CHIEF STATE SANITARY INSPECTOR OF THE RUSSIAN FEDERATION dated 16 September 2013 N 44 „On approval of SanPiN 2.6.1.3106-13 „Hygienic requirements for provision of radiation safety when using X-ray scanners for security checks of people., (2013)
- [49] C. Ronda. *Opt. Mater. X.* **22**, 100293 (2024). DOI: 10.1016/j.omx.2024.100293
- [50] P.A. Rodnyi. *Opt. Spectrosc.*, **107** (2), 270 (2009). DOI: 10.1134/S0030400X09080177
- [51] L. Jiang, D. Jiyang, H. Xinyou. *J. Inorg. Mater.*, **36** (8), 789 (2021). DOI: 10.15541/jim20200544
- [52] K. Taguchi, J.S. Iwaczyk. *Medical Physics.*, **40** (10), 100901 (2013). DOI: 10.1118/1.4820371
- [53] A. Esquivel, A. Ferrero, A. Mileto, F. Baffour, K. Horst, P.S. Rajiah, A. Inoue, S. Leng, C. McCollough, J.G. Fletcher. *Korean J. Radiol.*, **23** (9), 854. DOI: 10.3348/kjr.2022.0377
- [54] Y. Kudo, N. Ikeda. *Video-Assisted Thoracic Surgery*, **0** (4), 268 (2019). DOI: 10.21037/vats.2019.01.02
- [55] A. Pourmorteza, R. Symons, V. Sandfort, M. Mallek, M.K. Fuld, G. Henderson, E.C. Jones, A.M. Ashkan, L.R. Follo, D.A. Blumke. *Radiology*, **279** (1), 239 (2016). DOI: 10.1148/radiol.2016152601
- [56] M.T. Vervoorn, M. Wulfse, F.A.A. Mohamed Hoesein, M. Stellingwerf, N.P. van der Kaaij, L.M. de Heer. *Front Surg.*, **26** (9), 1079857 (2022). DOI: 10.3389/fsurg.2022.1079857
- [57] T.F. Budinger. *J. Nucl. Med.*, **24**, 73 (1983).
- [58] M. Conti, B. Bendriem. *Clinical and Translational Imaging*, **7**, 139 (2019). DOI: 10.1007/s40336-019-00316-5
- [59] M. Korjik, V. Alenkov, A. Borisevich, O. Buzanov, V. Dormenev, G. Dosovitskiy, A. Dosovitskiy, A. Fedorov, D. Kozlov, V. Mechinsky, R.W. Novotny, G. Tamulaitis, V. Vasiliev, H.-G. Zaunick, A.A. Vaitkevicius. *Nucl. Instrum. Meth. A.*, **871**, 42 (2017). DOI: 10.1016/j.nima.2017.07.045
- [60] A. Fedorov, A. Bondarau, A. Dzhurik, V. Bogomolov, A. Iyudin, Yu. Kashchuk, V. Mechinsky, S. Obudovsky, S. Svertilov, Y. Wu, D. Yanushevich, M. Korzhik. *Nucl. Instrum. Meth. A.*, **1062**, 169155 (2024). DOI: 10.1016/j.nima.2024.169155
- [61] E. Gordienko, A. Fedorov, E. Radiuk, V. Mechinsky, G. Dosovitskiy, E. Vashchenkova, D. Kuznetsova, V. Retivov, A. Dosovitskiy, M. Korjik, R. Sandu. *Opt. Mater.*, **78**, 312 (2018). DOI: 10.1016/j.optmat.2018.02.045

*Translated by T.Zorina*